Article

Polarization-Insensitive Graphene Modulator Based on Hybrid Plasmonic Waveguide

Songyue Liu [1]**, Manzhuo Wang** [1]**, Tingyu Liu** [1]**, Yan Xu** [1]**, Jianbo Yue** [1]**, Yunji Yi** [2] **, Xiaoqiang Sun** [1,*] **and Daming Zhang** [1]

1 State Key Laboratory of Integrated Optoelectronics, College of Electronic Science & Engineering, Jilin University, Changchun 130012, China

2 College of Integrated Circuits and Optoelectronic Chips, Shenzhen Technology University, Shenzhen 518000, China

* Correspondence: sunxq@jlu.edu.cn; Tel.: +86-136-0430-4384

Abstract: A polarization-insensitive graphene-assisted electro-optic modulator is proposed. The orthogonal T-shaped metal slot hybrid plasmonic waveguide allows the polarization-independent propagation of transverse electric field mode and complex mode. By the introduction of dual-layer graphene on the ridge waveguide, the polarization-insensitive modulation depths of the TE mode and complex mode are 0.511 dB/μm and 0.502 dB/μm, respectively. The 3 dB bandwidth of the modulator we have proposed is about 127 GHz at the waveguide length of 20 μm. The power consumption of 72 fJ/bit promised potential graphene electro-optic modulator applications for on-chip interconnected information transfer and processing.

Keywords: graphene; hybrid plasmonic waveguide; EO modulator; polarization-insensitive

1. Introduction

An electro-optical modulator is an important device in an optical fiber network and photonics integrated circuit [1]. EO modulators based on the bulk or thin-film LiNbO3 technology are mature but are still facing the challenges of relatively large size and high modulation voltage [2]. Though the fabrication of modulators based on silicon is perfectly compatible with the CMOS process, the limited EO coefficient leads to the low modulation efficiency [3]. The III-V semiconductor modulators offer a compact size, but the insertion loss (IL) and the stability are still not enough for practical applications [4]. Due to the intrinsic material characteristics, nonlinear polymer-based modulators have the merits of high EO coefficient, low driving voltage, and low dispersion [5]. However, their favorable performance largely depends on the high performance of poled EO polymer, which is obtained from a complex synthetizing process with low productivity. In addition, the reliability is yet to be proven in practical applications [6].

Graphene is a single-layer two-dimensional honeycomb lattice structure with excellent optoelectronic properties, such as an ultra-wide transmission spectral range, a tuning effect of light absorption, and high electronic conductivity and modulation rates. In addition, the Fermi level of graphene can be tuned by the applied voltage, thereby adjusting the absorption [7]. In 2011, the first graphene electro-optic modulator was experimentally fabricated. Its modulation depth (MD, which we define as the difference between the "on state" and the "off state") was 0.1 dB/μm [8]. After that, a modulator using graphene to form a double-layer flat capacitor was fabricated. The modulation depth was increased to 0.16 dB/μm [9]. Due to the strong mode confinement, the surface plasmon effect has also been introduced into graphene modulators [10,11]. Huang et al. proposed a waveguide-coupled hybrid plasmonic graphene modulator with a wide 3 dB bandwidth that can reach 0.48 THz and a power consumption of about 145 fJ/bit [12], which proves the privilege of a graphene-based hybrid plasmonic waveguide modulator. However, due to the feature of

atomic thickness, graphene-based modulators are sensitive to the polarization [13], which implies the independent modulation of the TE mode, transverse magnetic field (TM) mode, or TE-TM complex mode. The simultaneous modulation of both the TE mode and the TM mode is still to be implemented with a new waveguide [14,15].

In this paper, we propose a modulator based on a T-shaped metal slot waveguide and graphene to support the simultaneous modulation of both the TE mode and the TE-TM complex mode. Dual-layer graphene covers the top and one sidewall of the ridge waveguide. The finite element method is used study and optimize the geometric dimensions with respect to the equal modulation of the TE mode and the TE-TM complex mode. The simulation results show that the TE mode and the complex mode can be modulated at the depth of 0.511 dB/μm and 0.502 dB/μm, respectively. The 3 dB bandwidth of this modulator that we have proposed is about 127 GHz at the modulation length of 20 μm.

2. Device Structure

2.1. Hybrid Plasmonic Slot Waveguide

The proposed graphene modulator with a T-shaped hybrid plasmonic slot waveguide is shown in Figure 1. The device design and simulations are performed at the center wavelength of λ = 1550 nm. Three silver blocks (Ag, n_{Ag} = 0.14447 + 11.366i) and a sandwiched silicon oxide (SiO$_2$, n_{SiO2} = 1.45) insulator construct the orthogonal horizontal T-shaped slot waveguide. Dual 0.33 nm-thick graphene sheets isolated by hexagonal boron nitride (hBN, n_{hBN} = 1.98) with a thickness of 10 nm cover the top and one sidewall of the plasmonic waveguide. Two metal contacts connect the lower and the upper graphene sheet to the external voltage source, respectively [16]. The whole structure is supported by the SiO$_2$ substrate. The refractive index varies with the wavelength change. Therefore, the real part and imaginary part of the effective refractive index of Ag is confirmed at each wavelength by introducing the interpolation function to offer the precise result in the simulations.
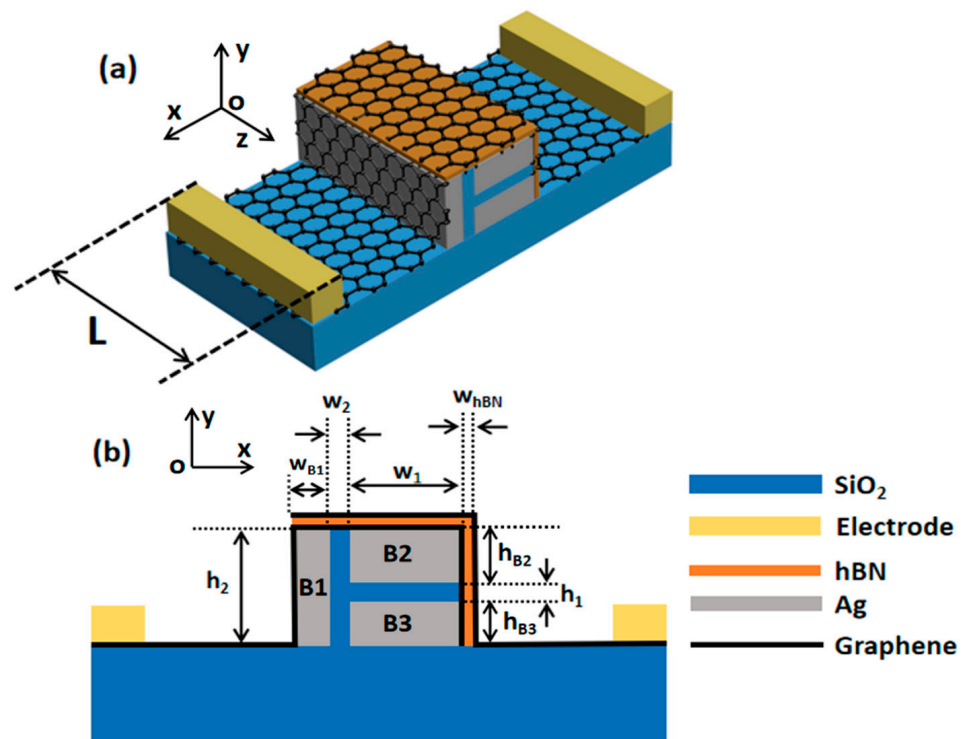
Figure 1. (**a**) Three-dimensional schematic diagram of graphene modulator based on metal slot waveguide; (**b**) Two-dimensional cross-sectional view of graphene modulator.

Our proposed dual built-in orthogonal slot waveguide can support two polarizations simultaneously, which overcomes the limitation of the polarization dependence of the common plasmonic waveguides. As shown in Figure 1, the T-shaped metal slot waveguide supports two modes with different polarizations. As shown in Figure 2, *E*x and *E*y represent the electric field distribution of the TE mode and the TE-TM complex mode, respectively. As shown in Figure 2a, at the optical wavelength of 1550 nm, the TE mode mainly exists in the vertical Ag slot, which is due to the surface plasmon excitation by the B1 and B2 Ag blocks [17]. The complex mode mainly exists in the horizontal slot, partially extending to the vertical slot waveguide, as shown in Figure 2b. Hence, the complex mode can be viewed as a mixed plasmonic mode generated in perpendicular metal slits.
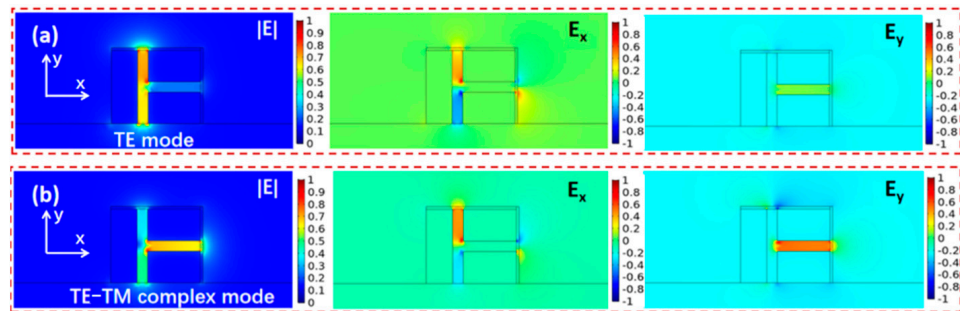
Figure 2. Electric field distributions of (**a**) TE mode and (**b**) TE-TM complex mode at the optical wavelength of 1550 nm.

To better evaluate the performance of the proposed modulator, the parameters of mode power attenuation (MPA), modulation depth (MD), and propagation loss (PL) are introduced. Here, MPA, MD, and PL can be defined as:

$$\text{MPA} = 40\pi\left(\log_{10} e\right)\text{Im}\left(N_{eff}\right)\lambda \tag{1}$$

$$\text{MD} = \text{MPA(OFF)} - \text{MPA(ON)} \tag{2}$$

$$\text{PL} = \text{MPA(ON)} \tag{3}$$

In the above equation, λ is the incident wavelength, Im (N_{eff}) is the imaginary part of the effective refractive index, the modulation depth is defined as the difference between mode power attenuation ("OFF" state) and mode power attenuation ("ON" state), and propagation loss refers to mode power attenuation ("ON" state).

2.2. Graphene Film

Graphene is a novel material with a two-dimensional single-layer honeycomb lattice structure. This unique feature offers graphene controllable optical absorption, considerable carrier mobility, 2.3% uniform optical absorption in a wide band, and other optical properties [18,19]. As shown in Figure 1, the 10 nm-thick hBN is sandwiched by two graphene films, which forms a plate capacitor. The applied bias voltage changes the Fermi level of the graphene and then the light absorption. The intrinsic tuning mechanism is consistent with that of the single-layer graphene modulator. The main difference is the capacitor structure that is constructed by the upper-layer graphene, lower-layer graphene, and the sandwiched hBN insulator.

In simulation, graphene can be defined either as a three-dimensional material with very thin thickness or as a two-dimensional structure without thickness [20]. In 3D model simulations, a fine mesh is demanded to obtain an accurate result, which implies long calculations and low efficiency. Therefore, the 2D model, which could provide similar accuracy and be more efficient, is adopted in this work. In this model, the graphene layer is considered as a surface conductive medium without thickness. In practical simulations, the performance of the modulator is mainly affected by the conductivity, and the conductivity

is mainly determined by the Fermi level, μ_c, the optical frequency, ω, and the relaxation time, τ, according to the Kubo formula [21,22]. The Fermi level, μ_c, as well as the surface conductivity, σ_g, are tuned by applying an external voltage. When no voltage or a low voltage is applied, the graphene behaves like metal, with high light absorption, which corresponds to the "OFF" state. However, when a certain voltage is applied, graphene behaves like a dielectric material, which corresponds to the "ON" state. Equation (1) illustrates the relationship between the Fermi level and the applied voltage [23]:

$$\mu_c = \hbar v_F \sqrt{\pi \eta \left| V_g - V_0 \right|} \tag{4}$$

where v_F is the Fermi velocity of graphene ($v_F = 2.5 \times 10^6$ m/s) [24] and η is determined by the insulation and thickness of hBN. As shown in Figure 3 below, μ_c can be changed from 0.2 to 0.6 eV as the applied bias voltage changes from 0.325 to 2.915 V.
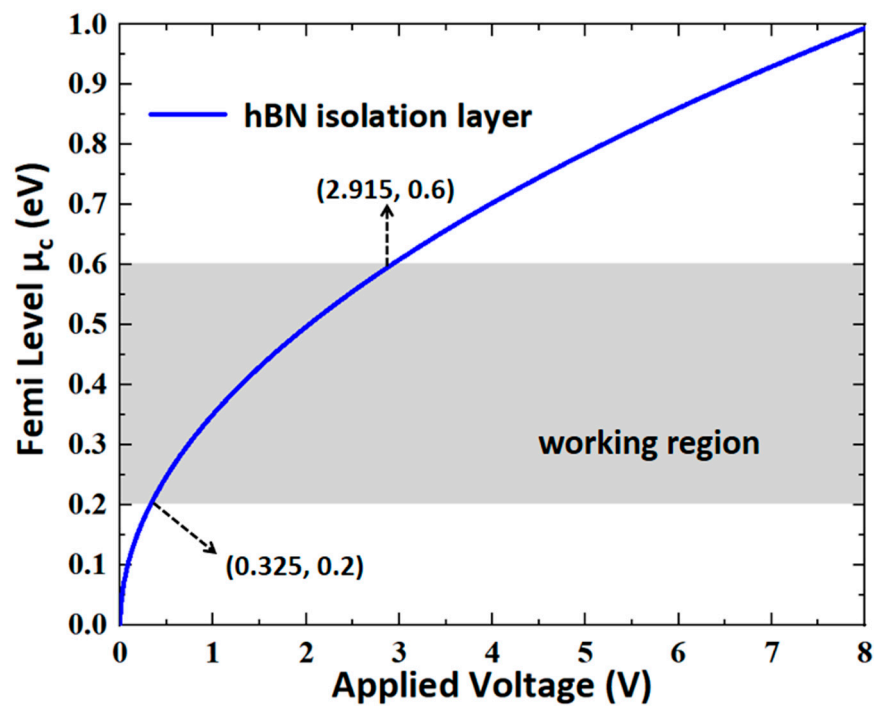

Figure 3. Graphene's Fermi level variation with applied voltage.

3. Design and Optimization

To confirm the influence of the waveguide dimensions on the mode distribution, simulations based on the FDTD method were carried out. Based on Maxwell's equations in wave optics, the two-dimensional wave optics module in the software (Lumerical Ltd., Vancouver, BC V6E 2M6, CA) was chosen. The mode in the waveguide was first studied to obtain different polarizations. Then, parametric scanning and global calculation were performed to determine the optimal waveguide size by monitoring the mode field status and modulation performance. In this process, the wavelength was set to be $\lambda = 1550$ nm. The frequency, f_0, was determined by the light speed and the wavelength. The dielectric constant, ε, of hBN is $8.85424 \times 10^{-12} F/m$. Here, the modulation (MD) is defined as the difference between the mode power attenuation (MPA) values at $\mu_c = 0$ eV and $\mu_c = 1$ eV. The propagation loss (PL) is the power attenuation (MPA) at $\mu_c = 0$ eV.

3.1. w_1

The TE mode and the complex mode in this hybrid plasmonic waveguide can be regarded as orthogonal polarizations supported by the Ag-SiO$_2$-Ag structure. The Re(N_{eff}) of the TE mode as a changing relationship of the Ag block width, w_1, is shown in Figure 4a.

An unremarkable Re(N_{eff}) variation is observed, which can be attributed to the lateral TE mode confinement, which is insensitive to the width change of Ag block B2 and Ag block B3. Conversely, the complex mode distribution is constrained by the T-shaped metal slots. Therefore, the Re(N_{eff}) of the complex mode decreases with the increment in w_1, which is due to the enhanced light absorption occurring in the gap between Ag blocks B2 and B3, as shown in Figure 4b.
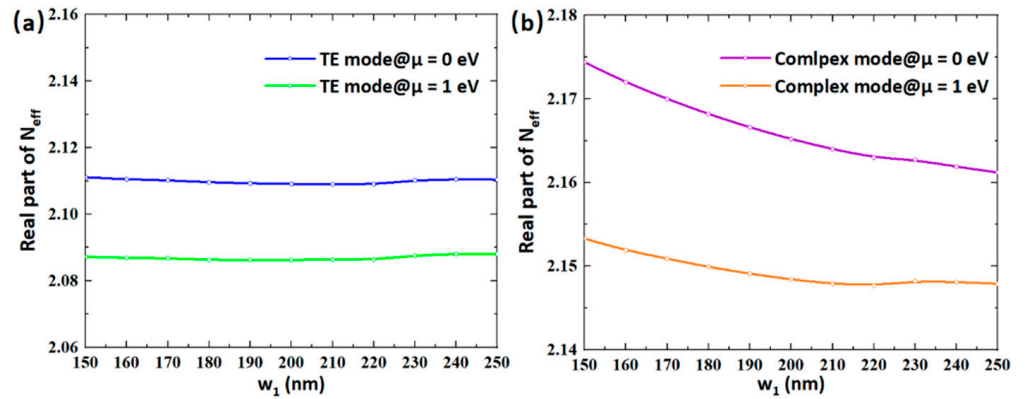

Figure 4. Re(N_{eff}) of (**a**) TE mode and (**b**) complex mode as a changing relationship of w_1.

As Figure 5 shows, for the TE mode, no significant MD and PL changes are observed. However, the MD and PL of the complex mode decrease with increases in w_1. To obtain the same MD, w_1 was chosen to be 200 nm, at which the real part of the effective index difference Re(ΔN_{eff}) of the TE and that of the complex modes are both around 0.05.
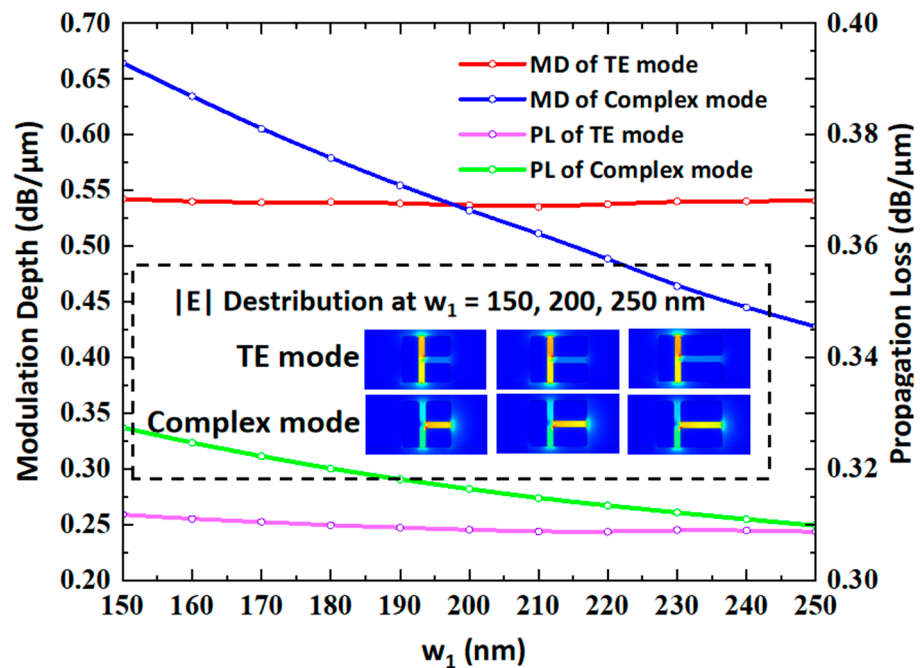

Figure 5. MD and PL of the TE mode and the complex mode as a changing relationship of w_1.

3.2. h_1

The height, h_1, of the horizontal slot largely affects the complex mode field distribution. Therefore, the Re(N_{eff}) of the TE mode, as a changing relationship of the Ag gap, h_1, is investigated. As Figure 6a shows, the limited Re(N_{eff}) change of the TE mode at different μ_c values is observed when h_1 varies from 35 to 45 nm. Conversely, the Re(N_{eff}) of the complex

mode decreases rapidly with the increment in h_1, which is due to the fast reduction in plasmonic mode confinement with increases in the metal gap distance.
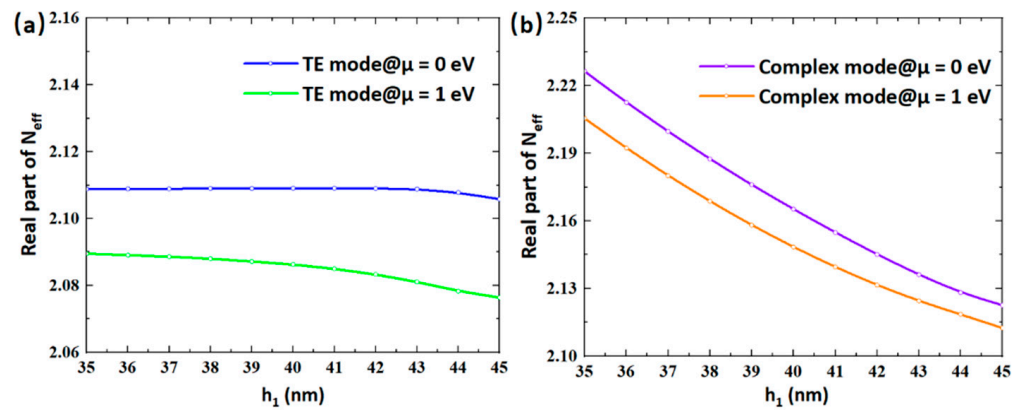

Figure 6. Re(N_{eff}) of (**a**) TE mode and (**b**) complex mode as a changing relationship of h_1.

The MDs of the TE mode and complex mode show inverse variations. The modulation depth of the TE mode rises with increases in h1, while the MD of the complex mode drops down as h_1 increases from 35 to 45 nm. The electric field distributions of the TE mode and the complex mode (h_1 = 35 nm and 40 nm) are shown in the insets of Figure 7. Due to the asymmetric waveguide structure, the enlargement of h_1 leads to the asymmetric distortion of the two modes. Moreover, the unbalanced placement of the graphene layers results in the inverse modulation when the metal gap, h_1, is increasing. However, the same MD can be obtained at h_1 = 40 nm. A similar scenario can be observed in the change in PL, and the same PL of the TE mode and complex mode is realized at h_1 = 41 nm. Therefore, h_1 was compromisingly chosen to be 40 nm.
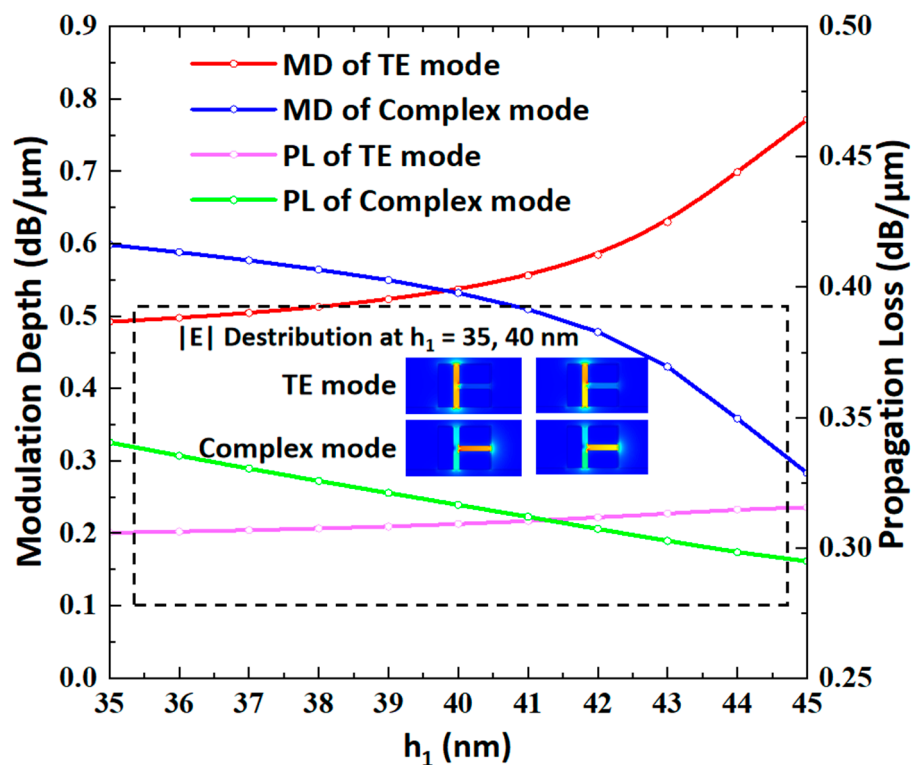

Figure 7. MD and PL of the TE mode and the complex mode as a changing relationship of h_1.

3.3. w_2

In this design, w_2 which is crucial for the restraint of the TE mode, refers to the gap size between Ag blocks B1 and B2 as well as B1 and B3. Similarly, the Re(N_{eff}) of the TE mode and the complex mode, as a changing relationship between the width of this slot, w_2, is investigated. As shown in Figure 8a,b, predictably, the Re(N_{eff}) decreases as w_2 varies from 35 to 45 nm, which is attributed to the weakening of the mode confinement. Consequently, the MD of the TE mode reduces with the increasing of w_2, as shown in Figure 9. For the complex mode, a stronger electric field can be observed at w_2 = 45 nm compared to that at w_2 = 35 nm. As a result, the MD of the complex mode increases with the increment in w_2. However, both modes have the same MD of about 0.53 dB/um at w_2 = 40 nm.
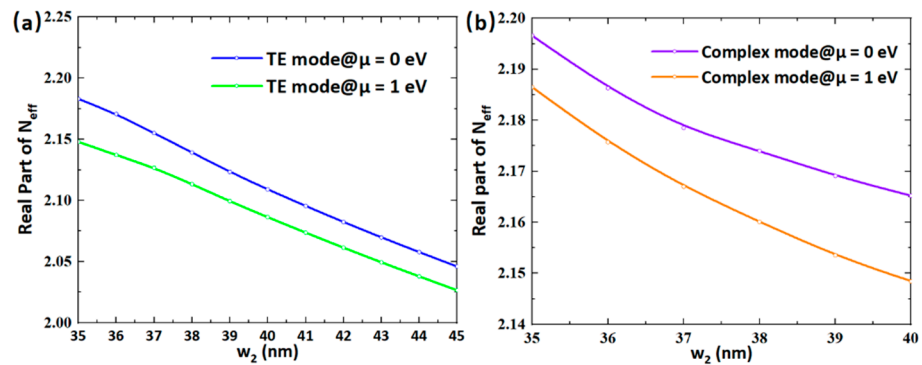

Figure 8. Re(N_{eff}) as a changing relationship of w_2 for (**a**) TE mode and (**b**) complex mode.
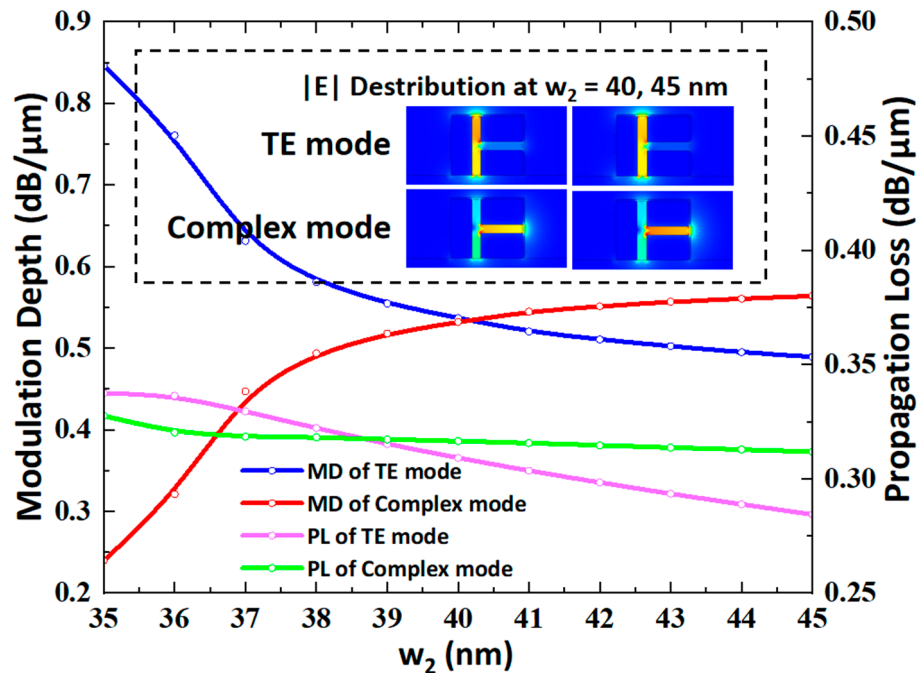

Figure 9. MD and PL of the TE mode and the complex mode as a changing relationship of w_2.

The PLs of both modes decrease when w_2 shifts from 35 to 45 nm, which is due to reduced mode penetration into the Ag block of B1. At w_2 = 40 nm, the PL difference between the two modes is about 0.01 dB/μm. For the purpose of polarization independence, w_2 was chosen to be 40 nm.

3.4. h_2

In Figure 1, h_2 represents the height of the proposed plasmonic waveguide. It is necessary to confirm the impact of h_2 on the characteristics of hybrid plasmonic waveguide

at $\mu_c = 0$ and $\mu_c = 1$ eV. As shown in Figure 10a, the Re(N_{eff}) of the TE mode gradually increases with increases in waveguide height, while the Re(N_{eff}) of the complex mode gradually declines with increases in h_2, as shown in Figure 10b.
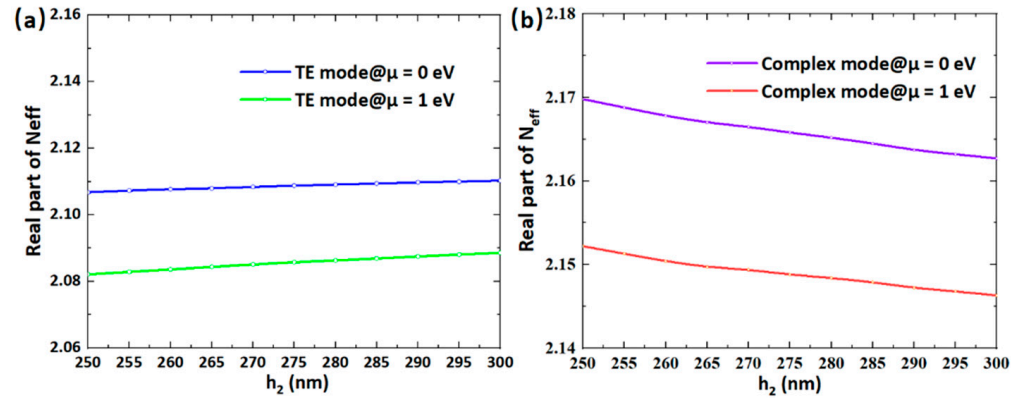

Figure 10. Re(N_{eff}) as a changing relationship of h_2 for (**a**) TE mode and (**b**) complex mode.

As Figure 11 shows, as h_2 varies from 250 to 300 nm, the MD difference between the two modes first shrinks then gradually expands. The same MD for the two modes can be obtained at $h_2 = 285$ nm. In addition, the increment in h_2 is accompanied by the gradual decrement of PL in both modes. The insets show the electric field distributions of the two modes at $h_2 = 250, 285,$ and 300 nm. At $h_2 = 285$ nm, the PL difference between two modes is about 0.005 dB/μm. Therefore, the hybrid waveguide height, h_2, was chosen to be 285 nm.
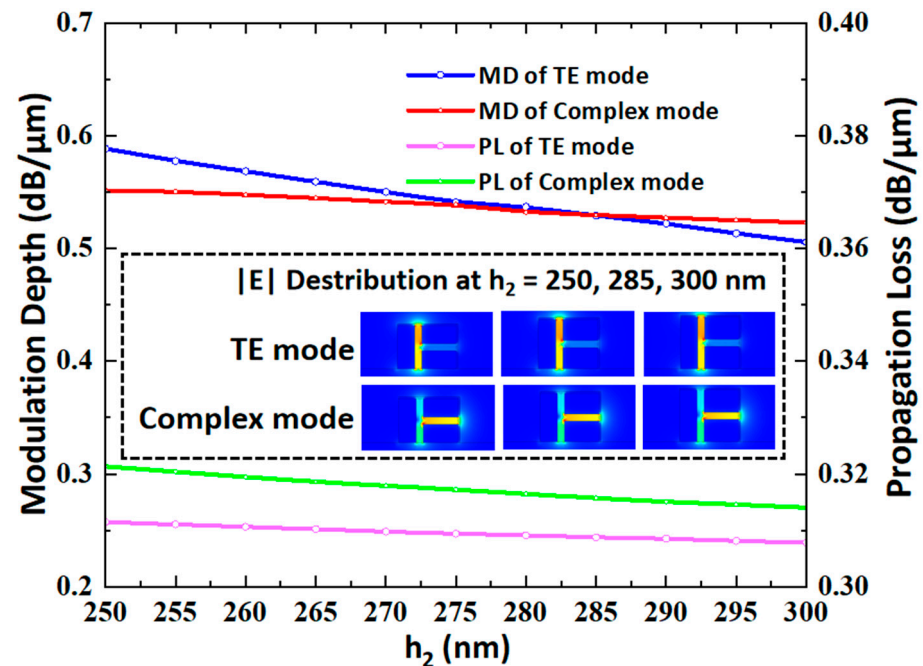

Figure 11. MD and PL as a changing relationship of h_2 for TE mode and complex mode.

3.5. w_{B1}

In this work, w_{B1} represents the width of the Ag block B1, as shown in Figure 1. Similarly, the Re(N_{eff}) of the TE mode and the complex mode all decrease when w_{B1} varies from 50 nm to 150 nm. As shown in Figure 12a,b, no obvious Re(N_{eff}) change happens when w_{B1} is larger than 100 nm.
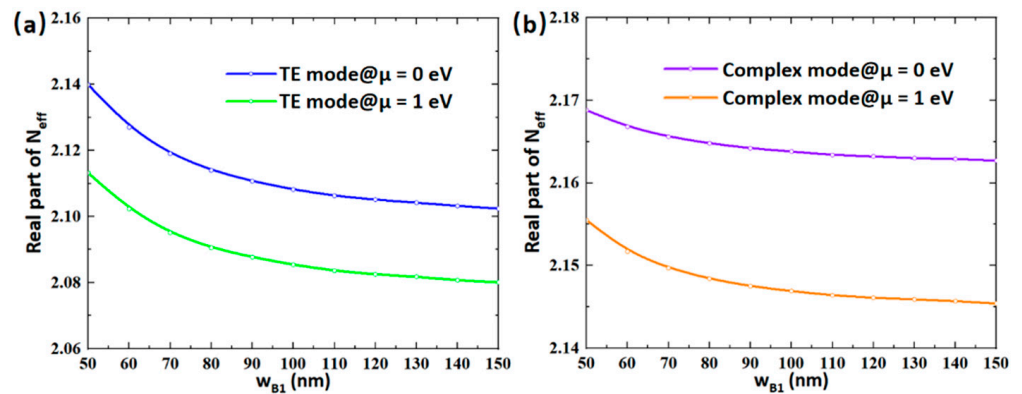
Figure 12. $\text{Re}(N_{\text{eff}})$ as a changing relationship of w_{B1} for (**a**) the TE mode and (**b**) the complex mode.

The MD and PL, as a changing relationship of w_{B1} for the TE mode and the complex mode, are shown in the Figure 13. The MD of the TE mode decreases as w_{B1} varies from 50 nm to 150 nm. Conversely, the MD of the complex mode increases when w_{B1} varies from 50 nm to 150 nm. The differences between the two modes first decrease then enlarge gradually. The same MD can be obtained at w_{B1} = 100 nm. The increment in w_{B1} is accompanied by the gradual decrement of PL for both modes. The insets in Figure 13 show the electric field distribution of the two modes at w_{B1} = 50, 100, and 150 nm. At w_{B1} = 100 nm, the PL difference between two modes is only about 0.005 dB/μm. With comprehensive consideration of MD, the hybrid waveguide height, w_{B1}, was chosen to be 100 nm.
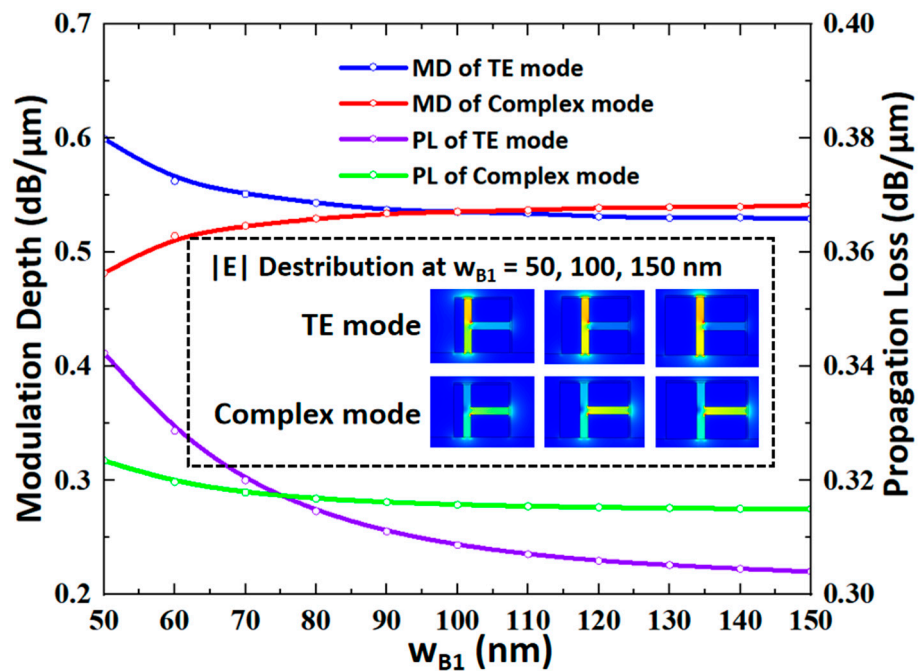

Figure 13. MD and PL as a changing relationship of w_{B1} for TE mode and complex mode.

3.6. h_{B2} and h_{B3}

The height of Ag blocks B2 and B3 may have an influence on the performance of the modulator. Because of the complete height of the plasmonic slot waveguide, h_2 is stable. When h_{B2} is increasing, the height of block B3 decreases accordingly. Therefore, the confirmation of h_{B2} would give the answer to h_{B3}. As shown in Figure 14, $\text{Re}(N_{\text{eff}})$ is investigated as a changing relationship of h_{B2} for the TE mode and the complex mode. When h_{B2} varies from 70 nm to 170 nm, the fluctuation in the $\text{Re}(N_{\text{eff}})$ of the TE mode is

only around 0.002 at $\mu_c = 0$ eV. At $\mu_c = 1$ eV, the Re(N_{eff}) of the TE mode gradually rises from 2.084 to 2.088. In comparison, the Re(N_{eff}) of the complex mode primarily drops when h_{B2} is lower than 105 nm then rises up again.

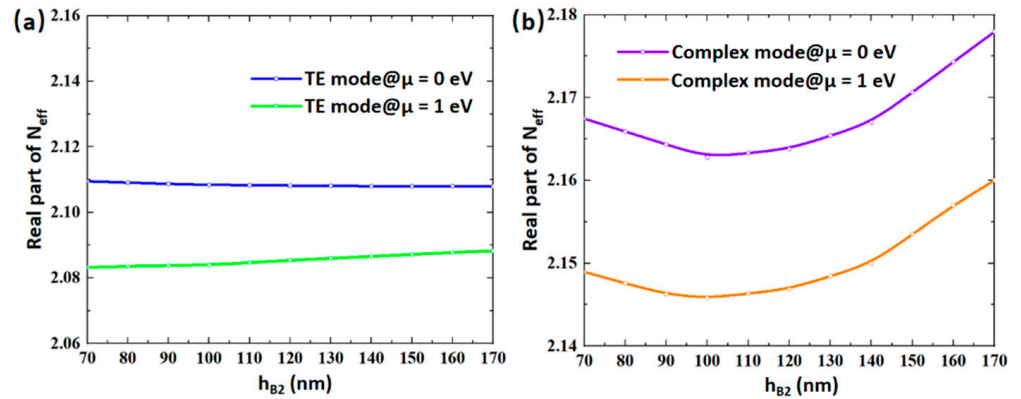**Figure 14.** Re(N_{eff}) as a changing relationship of h_{B2} for (**a**) TE mode and (**b**) complex mode.

As shown in Figure 15, the MDs of the TE mode and the complex mode gradually decrease. The same MD value for two modes can be obtained at $h_{B2} = 120$ nm. As h_{B2} increases, the PL of the TE mode monotonously decreases. The smallest PL difference between the two modes is 0.005 dB/μm at $h_{B2} = 100$ nm. The PL difference is about 0.007 dB/μm at $h_{B2} = 120$ nm. The insets show the electric field distributions of the TE mode and the complex mode at $h_{B2} = 100$, 120, and 160 nm. To obtain better polarization independence, h_{B2} was set to be 120 nm. Since h_2 is 285 nm, h_1 is 40 nm, and h_{B2} is 120 nm, h_{B3} was set to be 125 nm.
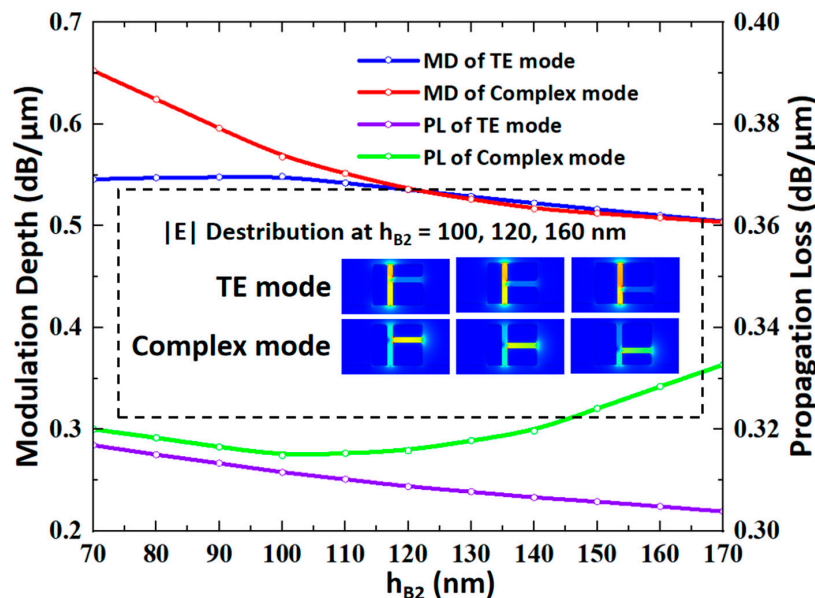

Figure 15. MD and PL as a changing relationship of h_{B2} for TE mode and complex mode.

4. Performance and Discussion

4.1. μ_c

After the confirmation of the geometric dimensions, the relationship between the modulation performance and the Femi level, μ_c, was investigated. As Figure 16 shows, when μ_c rises to 0.4 eV, the Re(N_{eff}) values of the TE mode and the complex mode reach maximums of 2.1742 and 2.1142, respectively. As μ_c shifts to 0.6 eV, the Re(N_{eff}) values of the TE mode and the complex mode gradually reduce to 2.1601 and 2.1012, respectively. At $\mu_c = 0.6$ eV, Re(ΔN_{eff}) is only 0.06.
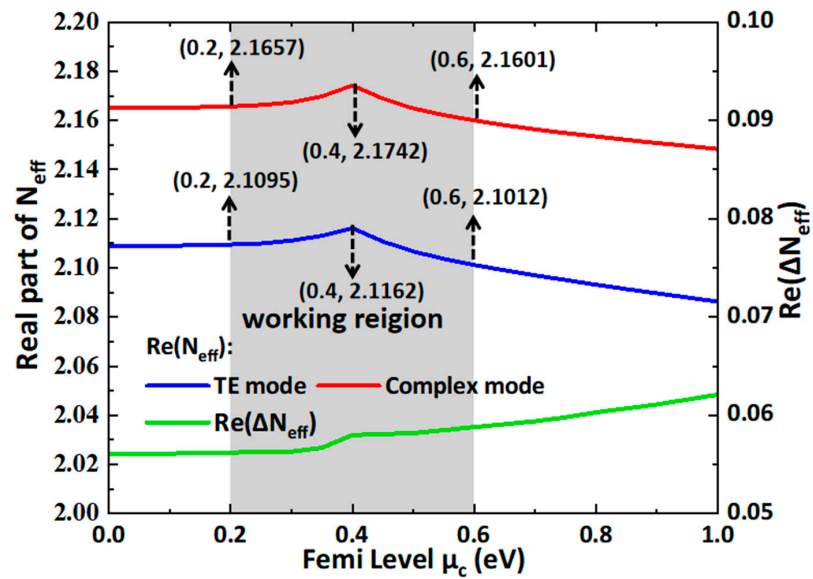
Figure 16. Re(N_{eff}) and Re(ΔN_{eff}) of the TE mode and the complex mode versus Femi level, μ_c.

As shown in Figure 17, a sharp drop in PL can be observed with the μc increasing from 0.2 eV to 0.6 eV. Therefore, we define the "ON" state at μ_c= 0.6 and the "OFF" state at μ_c = 0.2 eV. In this case, the MDs of the TE mode and the complex mode are 0.502 dB/μm and 0.511 dB/μm, respectively. The difference between $MD_{TE\text{-}mode}$ and $MD_{complex\ mode}$ is only 0.007 dB/μm at λ = 1550 nm.
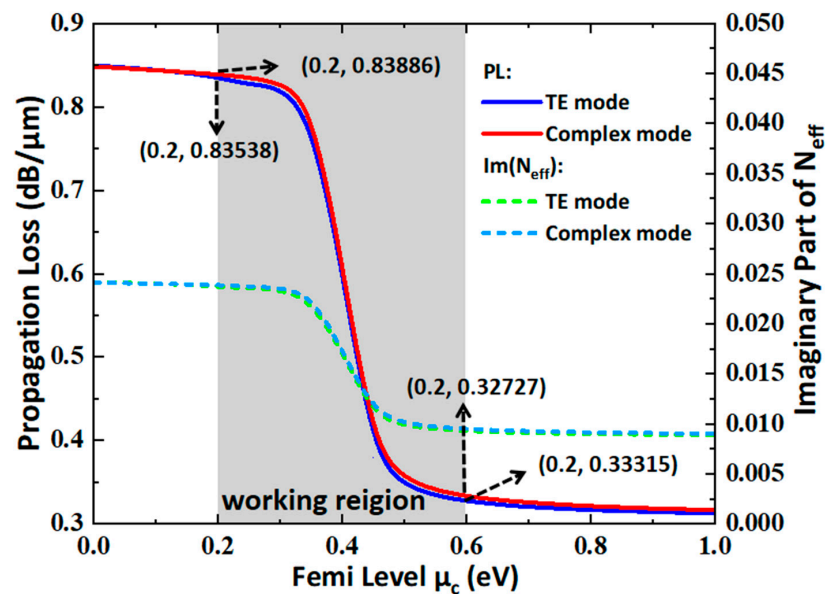

Figure 17. PL and Im(N_{eff}) of TE mode and complex mode versus Femi level, μ_c.

4.2. Optical Bandwidth

The optical bandwidth, as a changing relationship of the optical wavelength, was investigated with the Fermi level, μc, increasing from 0.2 eV to 0.6 eV. As Figure 18 shows, Re(N_{eff}) decreases with increases in wavelength. At λ = 1.1 μm and μ_c = 0.6 eV, the maximum Re(N_{eff}) values of the TE mode and the complex mode are 2.1723 and 2.2294, respectively. At λ = 1.1 μm and μ_c = 0.2 eV, the Re(N_{eff}) values of the TE mode and the complex mode are 2.1684 and 2.2238, respectively. At λ = 1.9 μm and μ_c = 0.6 eV, the Re(N_{eff}) values of the TE mode and the complex mode are 2.0762 and 2.1394, respectively. At λ = 1.9 μm and μ_c = 0.2 eV, the Re(N_{eff}) values of the TE mode and the complex mode

are 2.0942 and 2.1524, respectively. The Re(ΔN_{eff}) is no larger than 0.005 as the wavelength varies between 1.1 and 1.9 μm, which offers polarization independence to the TE mode and the complex mode.

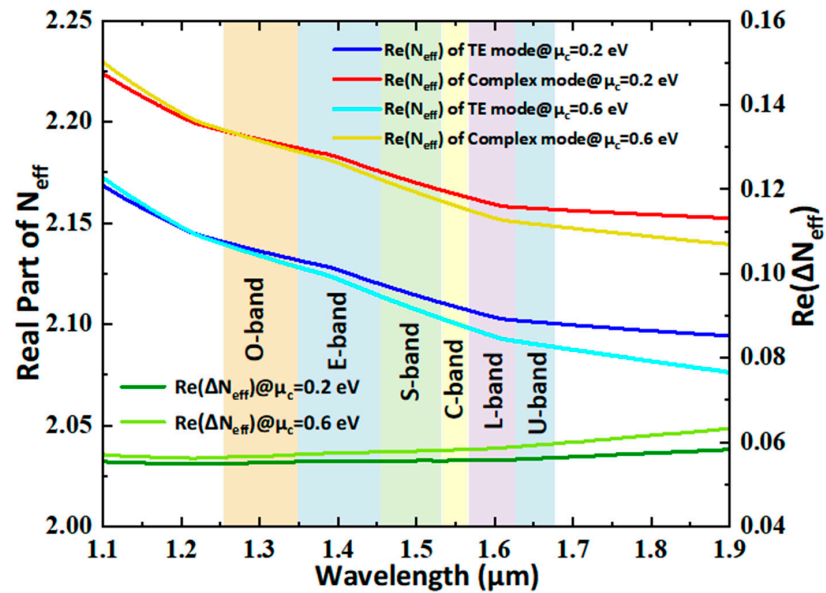**Figure 18.** Re(N_{eff}) and Re(ΔN_{eff}) of the TE mode and the complex mode vary with wavelength.

At $\mu_c = 0.2$ eV, the Im(N_{eff}) of the TE mode varies from 0.01613 to 0.02869 when the wavelength varies from 1.1 to 1.9 μm, as shown in Figure 19. Meanwhile, the Im(N_{eff}) of the complex mode increases from 0.01655 to 0.02897, which mainly results from the enhancement of the graphene–light interaction due to the increasing dielectric constant with increases in wavelength. The MPA change of both modes is very limited within the wavelength range. The MDs of the TE mode are 0.43145 dB/μm and 0.48145 dB/μm at $\lambda = 1.1$ μm and 1.9 μm, respectively. Similarly, the MDs of the complex mode are 0.47636 dB/μm and 0.49797 dB/μm at $\lambda = 1.1$ μm and 1.9 μm, respectively. The proposed device exhibits better polarization independence at longer wavelengths.

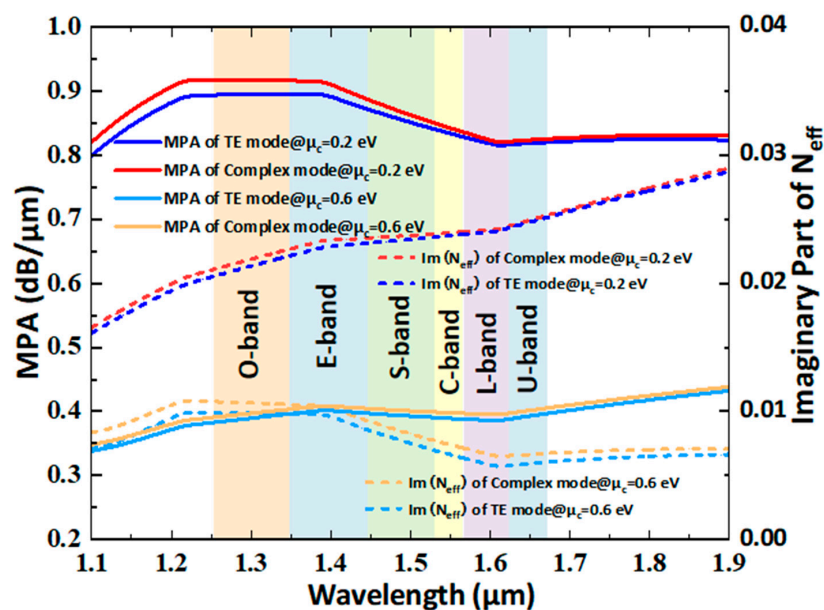**Figure 19.** Im(N_{eff}) and MPA of the TE mode and the complex mode vary with wavelength.

4.3. Frequency Response and Power Consumption

To calculate the frequency response and power dissipation, we made the modulator model equivalent to the circuit model, which is shown in Figure 20, and the dynamic response and power consumption of the proposed modulator were investigated. Here, C_{air}, which is composed of two electrodes and the air is around 12 fF [25]. The capacitor, *C*, consists of dielectric capacitance, C_D, and the quantum capacitance, C_Q. In simulation calculations, we consider graphene to be undoped, and we set the quantum capacitance to $C_Q = 0$. Therefore, the capacitor, *C*, can be represented by:

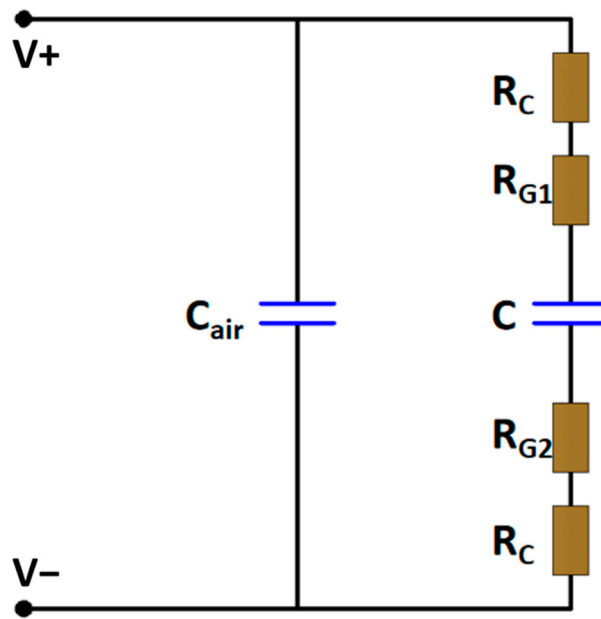$$C = \varepsilon_r \varepsilon_0 w_{ol} L / d \tag{5}$$

Figure 20. Equivalent circuit model for the estimation of bandwidth.

In Equation (5), *L* is the modulation length of this modulator, while w_{ol} = 620 nm represents the overlap width of dual-layer graphene. ε_r and *d* are the permittivity and thickness of the hBN isolation layer. The total resistance, R_{total}, is composed of the sheet resistance, R_S, of graphene and the resistance, R_c, which is composed by metal–graphene contact. Here, R_s and RC can be set as 100 $\Omega/\square$[26] and 100 Ω-μm [16], respectively. The total resistance, R_{total}, can be calculated by [27]:

$$R_{total} = R_s \times \frac{w_{g1} + w_{g2}}{L} + \frac{2R_c}{L} \tag{6}$$

where w_{g1} is 1120 nm and w_{g2} is 1400 nm. Then, R_{total} is 28.9 Ω. Theoretically, the 3 dB bandwidth ($f_{3\text{-dB}}$) of the proposed modulator is determined by the delay effect of the resistors and capacitors. Hence, $f_{3\text{-dB}}$ can be evaluated by [28]:

$$f_{3dB} = \frac{1}{2\pi R_{total} C_{total}} \tag{7}$$

With above optimized parameters, the bandwidth is around 127 GHz. When the modulation length, *L*, is 20 μm and the applied bias voltage varies from 0.325 V to 2.915 V (ΔU = 2.59 V), the power consumption can be estimated by:

$$E_{bit} = C_{total} (\Delta U)^2 / 4 \tag{8}$$

Then, we have an E_{bit} of 0.072 pJ/bit.

4.4. Discussion

To clarify the merits of proposed design, the theoretical performances of the polarization-insensitive graphene modulators that have been reported are comprehensively compared with that of this work. As shown in Table 1, the device we proposed has a higher bandwidth and $f_{3\text{-dB}}$ as well as the smallest E_{bit} compared to those proposed in other studies. Moderate MD and ΔMD values can also be obtained. The characteristics of $\mathrm{Re}(\Delta N_{eff})$ are also better than in most reported works. These favorable characteristics mainly originate from the hybrid waveguide structure, which provides a balanced mode field. The metal slot that supports the plasmonic mode offers the opportunity for wideband operation. It exhibits the favorable features of a small footprint, high speed, and low power consumption.

Table 1. Modulator performance comparison with reported works.

Ref.	Bandwidth (nm)	Re(ΔNeff)	MD (dB/µm)	ΔMD (dB/µm)	f3dB (GHz)	Ebit (fJ/bit)
[29]	1500–1600	-	0.06	0	13.4	-
[30]	1500–1600	-	0.08	0	80	-
[31]	1200–1600	-	mode A: 1.05, mode B: 1.13, mode C: 0.52	Min: 0.08 Max: 0.61	95	138.8
[32]	1530–1565	4.7×10^{-3}	TM mode: ~0.2975, TE mode: ~0.2895	~8×10^{-3}	30.2	2980
[33]	1367–1771	~0.5	TM mode: 1.113, TE mode: 1.119	~6×10^{-3}	6.1	7800
[34]	1450–1650	~0.1	TM mode: 1.392, TE mode: 1.347	0.045	~100	-
[35]	1300–1800	1.2×10^{-3}	-	-	135.6	-
This work	1100–1900	5×10^{-2}	TE mode: 0.511, complex mode: 0.502	0.009	127	72

5. Conclusions

A polarization-insensitive graphene-assisted electro-optic modulator is proposed. The orthogonal T-shaped metal slot structure offers polarization insensitivity. The proposed dual-layer graphene structure could enhance the light interaction and reduce the effective width of graphene, which is favorable for increasing bandwidth and reducing power consumption. Simulations with finite element algorithms show that the modulation depths of the TE mode and the complex mode supported by the proposed modulator are 0.502 dB/µm and 0.511 dB/µm, respectively. The 3 dB bandwidth is about 127 GHz when the modulation length is 20 µm. The power consumption may be restrained to 72 fJ/bit. The proposed modulator with a favorable bandwidth and relatively low power consumption has potential applications in high-speed on-chip interconnected information transfer and processing.

Author Contributions: The work described in this manuscript is a collaborative development of all authors. Conceptualization and resources: D.Z.; propose design and simulation optimization: S.L.; data verification: M.W.; data curation: T.L., Y.X., and J.Y.; funding acquisition and writing—review and editing: Y.Y. and X.S. All authors have read and agree to the published version of the manuscript.

Institutional Review Board Statement: No applicable.

Informed Consent Statement: No applicable.

Data Availability Statement: No applicable.

Conflicts of Interest: The authors declare no conflict of interest.

References

1. Bao, Q.; Loh, K.P. Graphene photonics, plasmonics, and broadband optoelectronic devices. *ACS Nano* **2012**, *6*, 3677–3694. [CrossRef] [PubMed]
2. Mercante, A.J.; Eng, D.L.K.; Konkol, M.; Yao, P.; Shi, S.; Prather, D.W. Thin LiNbO3on insulator electro-optic modulator. *Opt. Lett.* **2016**, *41*, 867–869. [CrossRef] [PubMed]
3. Pérez-Galacho, D.; Marris-Morini, D.; Stoffer, R.; Cassan, E.; Baudot, C.; Korthorst, T.; Boeuf, F.; Vivien, L. Simplified modeling and optimization of silicon modulators based on free-carrier plasma dispersion effect. *Opt. Express* **2016**, *24*, 26332–26337. [CrossRef]
4. Jin-Kown, P.; Shinichi, T.; Mitsuru, T. InGaAsP Mach-Zehnder interferometer optical modulator monolithically integrated with InGaAs driver MOSFET on a III-V CMOS photonics platform. *Opt. Express* **2018**, *26*, 4842–4852.
5. Qiu, F.; Yokoyama, S. Effiiciently poled electro-optic polymer modulators. *Opt. Express* **2016**, *24*, 19020–19025. [CrossRef]
6. Wang, X.; Jiang, M.; Sun, S.; Sun, J.; Yi, Y.; Chen, C.; Sun, X.; Wang, F.; Cui, Z.; Zhang, D. Demonstration of a high-speed electro-optic switch with passive-to-active integrated waveguide based on SU-8 material. *RSC Adv.* **2016**, *6*, 50166–50172. [CrossRef]
7. Wang, F.; Zhang, Y.; Tian, C.; Girit, C.; Zettl, A.; Crommie, M.; Shen, Y. Gate-variable optical transitions in graphene. *Science* **2008**, *320*, 206–209. [CrossRef]
8. Liu, M.; Yin, X.; Ulin-Avila, E.; Geng, B.S.; Thomas, Z.; Ju, L.; Wang, F.; Zhang, X. A graphene-based broadband optical modulator. *Nature* **2011**, *474*, 64–67. [CrossRef]
9. Liu, M.; Yin, X.; Zhang, X. Double-layer graphene optical modulator. *Nano Lett.* **2012**, *12*, 1482–1485. [CrossRef]
10. Gramotnev, D.K.; Bozhevolnyi, S.I. Plasmonics beyond the diffraction limit. *Nat. Photonics* **2010**, *4*, 83–91. [CrossRef]
11. Rakib Hasan, K.B.M.; Noman Sarker, M.A.; Islam, M.A.; Alam, M.S. Coupling Characteristics of Surface Plasmons in Coupled Elliptical Nanowires. *OSA Contin.* **2018**, *1*, 1414–1428. [CrossRef]
12. Huang, B.; Lu, W.; Li, X.; Wang, J.; Liu, Z. Waveguide-coupled hybrid plasmonic modulator based on graphene. *Appl. Optics* **2016**, *55*, 5598–5602. [CrossRef] [PubMed]
13. Bao, Q.; Zhang, H.; Wang, B.; Ni, Z.; Lim, C.; Yi, X.; Wang, Y.; Tang, D.; Loh, K.P. Broadband graphene polarizer. *Nat. Photonics* **2011**, *5*, 411–415. [CrossRef]
14. Okayama, H.; Onawa, Y.; Takahashi, H.; Shimura, D.; Sasaki, H. Polarization insensitive silicon waveguide wavelength filter using polarization rotator and mode conversion Bragg grating with resonator cavity. *Jpn. J. Appl. Phys.* **2020**, *59*, 128002. [CrossRef]
15. Chang, L.; Lei, L.; Gong, Y.; Tan, M.; Yu, Y.; Li, Z. Polarization-independent directional coupler and polarization beam splitter based on asymmetric cross-slot waveguides. *Appl. Optics* **2018**, *57*, 678–683. [CrossRef]
16. Zhong, H.; Zhang, Z.; Chen, B.; Xu, H.; Yu, D.; Huang, L.; Peng, L. Realization of low contact resistance close to theoretical limit in graphene transistors. *Nano Res.* **2015**, *8*, 1669–1679. [CrossRef]
17. Veronis, G.; Fan, S. Modes of Subwavelength Plasmonic Slot Waveguides. *J. Light. Technol.* **2007**, *25*, 2511–2521. [CrossRef]
18. Geim, A.K.; Novoselov, K.S. The rise of graphene. *Nat. Mater.* **2009**, *6*, 183–191. [CrossRef]
19. Avouris, P.; Chen, Z.; Perebeinos, V. Carbon Based Electronics. *Nat. Nanotechnol.* **2007**, *2*, 605–615. [CrossRef]
20. Ye, L.; Sui, K.; Zhang, Y.; Liu, Q. Broadband optical waveguide modulators based on strongly coupled hybrid graphene and metal nanoribbons for near-infrared applications. *Nanoscale* **2019**, *11*, 3229–3239. [CrossRef]
21. Pasanen, P.; Voutilainen, M.; Helle, M.; Song, X.; Hakonen, P.J. Graphene for future electronics. *Phys. Scr.* **2012**, *T146*, 014025. [CrossRef]
22. Stauber, T.; Peres, N.M.R.; Geim, A.K. Optical conductivity of graphene in the visible region of the spectrum. *Phys. Rev. B* **2008**, *78*, 085432. [CrossRef]
23. Sensale-Rodriguez, B.; Yan, R.; Kelly, M.M.; Fang, T.; Tahy, K.; Hwang, W.S.; Jena, D.; Liu, L.; Xing, H.G. Broadband graphene terahertz modulators enabled by intraband transitions. *Nat. Commun.* **2012**, *3*, 780–786. [CrossRef] [PubMed]
24. Hwang, C.; Siegel, D.A.; Mo, S.K.; Regan, W.; Ismach, A.; Zhang, Y.; Zettl, A.; Lanzara, A. Fermi velocity engineering in graphene by substrate modification. *Sci. Rep.* **2012**, *2*, 590–593. [CrossRef]
25. Hu, Y.; Xiao, X.; Xu, H.; Li, X.; Xu, K.; Li, Z.; Chu, T.; Yu, Y.; Yu, J. High-speed silicon modulator based on cascaded microring resonators. *Opt. Express* **2012**, *20*, 15079–15085. [CrossRef]
26. Shiramin, L.A.; Thourhout, D.V. Graphene Modulators and Switches Integrated on Silicon and Silicon Nitride Waveguide. *IEEE J. Sel. Top. Quantum Electron.* **2017**, *23*, 94–100. [CrossRef]
27. Koester, S.J.; Li, M. High-speed waveguide-coupled graphene-on-graphene optical modulators. *Appl. Phys. Lett.* **2012**, *100*, 171107. [CrossRef]
28. Zheng, P.; Yang, H.; Fan, M.; Hu, G.; Zhang, R.; Yun, B.; Cui, Y. A Hybrid Plasmonic Modulator Based on Graphene on Channel Plasmonic Polariton Waveguide. *Plasmonics* **2018**, *13*, 2029–2035. [CrossRef]
29. Yang, Z.; Lu, R.; Cai, S.; Wang, Y.; Liu, Y. A CMOS-compatible and polarization-insensitive graphene optical modulator. *Opt. Commun.* **2019**, *450*, 130–135. [CrossRef]
30. Yang, Z.; Lu, R.; Wang, Y.; Cai, S.; Zhang, Y.; Wang, X.; Liu, Y. A fabrication-friendly graphene-based polarization insensitive optical modulator. *Optik* **2019**, *182*, 1093–1098. [CrossRef]
31. Shirdel, M.; Mansouri-Birjandi, M.A. Broadband graphene modulator based on a plus-shaped plasmonic slot waveguide. *Appl. Optics* **2019**, *58*, 8174–8179. [CrossRef]
32. Hu, X.; Wang, J. Design of graphene-based polarization-insensitive optical modulator. *Nanophotonics* **2018**, *7*, 651–658. [CrossRef]

33. Xu, Y.; Li, F.; Kang, Z.; Huang, D.; Zhang, X.; Tam, H.Y.; Wai, P.K.A. Hybrid Graphene-Silicon Based Polarization-Insensitive Electro-Absorption Modulator with High-Modulation Efficiency and Ultra-Broad Bandwidth. *Nanomaterials* **2019**, *9*, 157. [Cross-Ref] [PubMed]
34. Ye, S.; Liang, D.; Lu, R.; Shah, M.; Zou, X.; Yang, F.; Yuan, F.; Liu, Y. Polarization Independent Modulator by Partly Tilted Graphene Induced Electro-Absorption Effect. *IEEE Photonics Technol. Lett.* **2016**, *29*, 23–26. [CrossRef]
35. Zou, X.; Zhang, Y.; Li, Z.; Yang, Y.; Zhang, S.; Zhang, Z.; Zhang, Y.; Liu, Y. Polarization-Insensitive Phase Modulators Based on an Embedded Silicon-Graphene-Silicon Waveguide. *Appl. Sci.* **2019**, *9*, 429. [CrossRef]